ASCE

Generalization and Analysis of Elastic Water Column Model for Hydraulic Transient Analysis of Water Distribution Systems

Morteza Imani[1]; Aaron Zecchin[2]; Wei Zeng[3]; and Martin F. Lambert, A.M.ASCE[4]

Abstract: The elastic water column model (EWCM) has been enhanced through the integration of dynamic electromechanical elements, such as pressure-reducing valves (PRVs) and pumps, facilitating advanced transient analysis of water distribution systems in the time domain. The graph-theoretical framework has been employed to represent any arbitrary network configuration with different hydraulic components. Electric equivalent circuits (EECs) have been introduced for these dynamic components and integrated to the EWCM create a set of differential algebraic equations (DAEs). Verification against established models, such as the rigid water column model (RWCM) and the method of characteristics (MOC), confirms the enhanced EWCM's accuracy, validity, and computational advantages. Specifically, in fast transient scenarios, the EWCM outperforms the RWCM by accounting for water compressibility. It also surpasses the MOC in computational efficiency due to its foundation on ordinary differential equations and independence from Courant–Friedrichs–Lewy condition constraints. The model's accuracy is controllable by increasing the number of reaches, although this increases computational cost. The investigation into the model's stiffness reveals a notable increase, with the EWCM being approximately 25 times stiffer than the RWCM. Although this allows for capturing a broader frequency range, it also increases numerical stiffness, making solver selection more critical. The study further emphasizes the computational advantages of employing sparse matrices within the EWCM. In large-scale networks, the graph representation of the EWCM predominantly features sparse matrices, which reduce computation time and memory usage. **DOI: [10.1061/JWRMD5.WRENG-6946](https://doi.org/10.1061/JWRMD5.WRENG-6946).** © 2025 American Society of Civil Engineers.

Author keywords: Elastic water column model (EWCM); Rigid water column model (RWCM); Stiffness; Graph theory; Pressure-reducing valves (PRVs).

Introduction

Hydraulic transients in water distribution systems (WDS) can be triggered by both rapid events and the gradual changes of dynamic elements, leading to a spectrum of transient responses. These transients are categorized into fast and slow types, with slow transients often generated by the controlled operation of dynamic components such as hydraulically controlled pressure-reducing valves (PRVs) and variable-speed pumps. For example, PRVs may take tens of seconds to a minute to adjust to a new position, and variable-speed pumps exhibit time constants of tens of seconds due to the combined inertia of the motor and pump, contributing to gradual pressure and flow changes ([Prescott and Ulanicki 2008](#)). However, under certain conditions, these same elements can also be sources of fast transients. A sudden stoppage of pumps, for instance, can cause a rapid reversal of flow, generating high-speed pressure waves, and a rapid operation or failure of a PRV can lead to sudden pressure spikes or drops. Such fast transients pose significant challenges, including the potential for pipe failures, underscoring the complexity of managing hydraulic behaviors in WDS ([Xing and Sela 2020](#)).

Effectively simulating both fast and slow transients requires a thorough characterization of unsteady flow to select appropriate models. Traditional methods like the method of characteristics (MOC) have been employed to predict specifically fast transient wave behavior, informing design processes and mitigation strategies. The scope of modeling fast transients extends beyond design to include fault detection ([Zeng et al. 2020](#), [2023](#)), condition assessment ([Zhang et al. 2020](#)), model calibration ([Simpson et al. 2000](#)), pressure management ([Creaco et al. 2017a](#), [b](#)), and uncertainty quantification ([Khilqa et al. 2019](#)).

Despite its utility, the MOC approach is computationally demanding, and satisfying the Courant–Friedrichs–Lewy (CFL) condition to ensure stable solutions limits its applicability for slow transients ([Nault and Karney 2016a](#)). To address this challenge, the rigid water column model (RWCM) was introduced, simplifying the partial differential equations (PDEs) of momentum and mass conservation for WDS into a set of ordinary differential equations (ODEs) by assuming an infinite wave speed ([Nault and Karney 2016b](#)). This model facilitates a larger time-step selection, making RWCM suitable for control and optimization purposes. Early RWC modeling, such as Onizuka's ([1981](#), [1986](#)) loop-based model for pipe networks developed between 1981 and 1986 extended steady-state flow analyses but was limited by the need

[1]Ph.D. Candidate, School of Architecture and Civil Engineering, Univ. of Adelaide, Adelaide, SA 5005, Australia. ORCID: https://orcid.org/0000-0002-1618-3740. Email: morteza.imani@adelaide.edu.au

[2]Senior Lecturer, School of Architecture and Civil Engineering, Univ. of Adelaide, Adelaide, SA 5005, Australia. ORCID: https://orcid.org/0000-0001-8908-7023. Email: aaron.zecchin@adelaide.edu.au

[3]Lecturer, School of Architecture and Civil Engineering, Univ. of Adelaide, Adelaide, SA 5005, Australia (corresponding author). ORCID: https://orcid.org/0000-0003-3525-0432. Email: w.zeng@adelaide.edu.au

[4]Professor, School of Architecture and Civil Engineering, Univ. of Adelaide, Adelaide, SA 5005, Australia. Email: martin.lambert@adelaide.edu.au

© ASCE   04025054-1   J. Water Resour. Plann. Manage.

J. Water Resour. Plann. Manage., 2025, 151(10): 04025054

for pseudoloops and fictitious flows. Shimada's (1989, 1992) introduction of the incidence matrix method in significantly enhanced modeling efficiency by accurately depicting network topology, facilitating slow transient event simulation without pseudoloops. This advancement broadened RWCM's applicability across various network configurations.

A significant milestone was achieved with the development of the Rigid Water Column Global Gradient Algorithm (RWC-GGA) by Nault and Karney (2016b), evolving from generalized global gradient algorithms to include inertial effects and considerations for variable-area tanks and node outflows, marking a notable improvement in RWCM methodology. The RWCM model further evolved by incorporating dynamic components like PRVs and pumps (Ulanicki and Beaujean 2021).

Despite its advancements in different aspects, RWCM faces significant numerical errors when simulating high-frequency water hammer waves (Zeng et al. 2022). To simulate fast transients and incorporate water compressibility while retaining the computational advantages of RWCMs, the elastic water column model (EWCM) was introduced. Initially applied in the hydropower field by Nicolet (2007), this model treats a pipe section as a lumped system. This approach has been successfully applied to stability analysis and transient simulation in hydropower stations, showcasing its utility and effectiveness (Nicolet et al. 2007; Souza et al. 1999; Zeng et al. 2015, 2016).

The development of the elastic water column (EWC) model was notably inspired by methodologies from the telecommunication sector, particularly the approach to resolving the propagation of electrical waves in conductors through an equivalent scheme (Jaeger 1977). This scheme offered a high level of abstraction and a rigorous formalism, encapsulated in the telegraphist's equations. The analogy between this and the momentum and continuity equations, which model the propagation of pressure waves in hydraulic systems, is striking. It facilitates the identification of a lineic hydraulic resistance (attributable to head losses through a pipe), a lineic hydraulic inductance (reflecting the inertia effect of water), and a lineic hydraulic capacitance (corresponding to the storage effect due to pressure increase and thus a function of the wave speed) (Nicolet 2007). Analyzing this equivalent scheme offers insights into both steady-state and transient conditions, revealing that in steady states, only the resistance is significant, causing head losses along the pipe.

In 2022, the EWCM was applied to pipe networks for the first time, combining a graph-theoretic approach with a distributed scheme electric equivalent circuit (EEC) to simulate hydraulic transients across various network components. This application demonstrated the method's ability to optimize both accuracy and efficiency in simulating hydraulic transient events in pipe networks (Zeng et al. 2022). Furthermore, a notable advantage of the EWC model is its foundation on ODEs, enabling its representation in a state-space format. This format is instrumental for conducting modal analysis, enabling stability and observability assessments, and supporting various other control applications, thus greatly enhancing the model's utility in the analysis and management of WDS.

This study aims to build upon the work of Zeng et al. (2022) by incorporating dynamic components such as PRVs and pumps into the EWCM, establishing a comprehensive framework for integrating any dynamic element into the model. In addition, the study rigorously evaluates the EWCM's performance under various conditions, comparing it with traditional models like the RWCM and the MOC, particularly in terms of handling higher frequency excitations in water networks. The stiffness and computational efficiency of the EWCM, especially in large-scale networks, are also examined by leveraging sparse matrices.

The "Methodology" section outlines the mathematical formulation of the EWCM and its integration with dynamic elements using EECs. The "Numerical Simulation" section follows with two case studies that compare the EWCM's performance with the RWCM and MOC for both slow and fast transients. Next, the "Numerical Considerations" section discusses key factors such as stiffness and sparsity, highlighting both the computational benefits and challenges of the EWCM for large systems. Finally, the "Conclusion" summarizes the findings and discusses potential applications and future directions for optimizing and controlling water distribution systems.

Methodology

The one-dimensional partial differential equations of momentum and continuity for a pressurized pipeline system are given as follows:

$$\frac{\partial h}{\partial x} + \frac{1}{gA}\frac{\partial q}{\partial t} + \frac{fq|q|}{2gDA^2} = 0 \qquad (1)$$

$$\frac{gA}{a^2}\frac{\partial h}{\partial t} + \frac{\partial q}{\partial x} = 0 \qquad (2)$$

where h = piezometric head; q = volumetric flow rate; g = gravitational acceleration; A = internal cross-sectional area of the pipeline; D = diameter of the pipe; and f = Darcy–Weisbach friction factor. In analyzing a distinct segment of pipe of length l, with the assumption of constant spatial gradients in hydraulic conditions (i.e., $\partial h/\partial x \approx \Delta h/l$ and $\partial q/\partial x \approx \Delta q/l$), the equations governing transient flow are reformulated as follows (Souza et al. 1999):

$$\Delta h = -L\frac{\partial q}{\partial t} - Rq|q| \qquad (3)$$

$$\Delta q = -C\frac{\partial h}{\partial t} \qquad (4)$$

where L = hydraulic inductance, which equals l/gA; C = hydraulic capacitance, which equals gAl/a^2; and R = hydraulic resistance, which is $fl/2gDA^2$.

Although it is theoretically ideal to distribute the flow rate change from water compressibility evenly along the pipeline, the electrical equivalent method (EEM) simplifies this by concentrating it at specific points within the pipe section. These points include the center (T-shape electrical circuit), upstream end, downstream end, or both ends of the pipe section (π-shaped electrical circuit). Zeng et al. (2022) explored these configurations, and this study specifically selects the π-shaped electrical circuit due to its efficiency in simulating the dynamic hydraulic behaviors in pipelines with high accuracy. For such an EEM configuration, equations for the jth pipe in the network are defined as follows:

$$L_j\frac{dq_j}{dt} = -R_j|q_j|q_j + (h_{j,u} - h_{j,d}) \qquad (5)$$

$$\frac{C_j}{2}\frac{dh_{j,u}}{dt} = \Delta q_{j,u} \qquad (6)$$

$$\frac{C_j}{2}\frac{dh_{j,d}}{dt} = \Delta q_{j,d} \qquad (7)$$

where subscript j = jth pipe (or reaches) in the network; and u and d = upstream and downstream ends, respectively. Given Eqs. (6) and (7), the continuity equation for a node—where multiple pipes

© ASCE

04025054-2

J. Water Resour. Plann. Manage.

may intersect, connect to a tank, or have a demand—can be expressed as follows:

$$\sum_{j\in\Lambda_{i,u}}q_j - \sum_{j\in\Lambda_{i,d}}q_j - \sum_{j\in\Lambda_{i,u}}\Delta q_{j,u} - \sum_{j\in\Lambda_{i,d}}\Delta q_{j,d} - Q_i = 0 \quad (8)$$

where t $\sum_{j\in\Lambda_{i,u}}q_i$ = total inflow to node i from the set of incoming pipes denoted as $\Lambda_{i,u}$; $\sum_{j\in\Lambda_{i,d}}q_j$ = total outflow from the node i to the set of outgoing pipes $\Lambda_{i,d}$; Q_i = demand at the node; and $\Delta q_{j,d}$ and $\Delta q_{j,u}$ = changes in flow rate at the node due to water compressibility and pipe elasticity, affecting the downstream and upstream pipes respectively. These changes are crucial for understanding the dynamics of fluid flow within the network, especially in response to variations in pressure and volume. The primary distinction between the EWCM and the RWCM lies in these two additional terms. Substituting Eqs. (6) and (7) into Eq. (8) to replace the compressibility terms and considering an extra capacitance T for having a tank at the node terms yields

$$\left(\frac{1}{2}\sum_{j\in\Lambda_i}C_j + T_i\right)\frac{dh_i}{dt} = \sum_{j\in\Lambda_{i,u}}q_j - \sum_{j\in\Lambda_{i,d}}q_j - Q_i \quad (9)$$

Eqs. (5) and (9) are the two fundamental equations for the EWCM, within which the dynamic elements such as PRVs and pumps will be incorporated.

Pressure-Reducing Valves

PRVs are modeled as a two-port component, analogous to a pipe, which facilitates its integration into hydraulic network simulations. This modeling approach simplifies the representation of PRVs, focusing on their connectivity between two nodes: the upstream node and the downstream node. The essential function of the PRV, under this paradigm, is to regulate the downstream pressure to a predetermined set point, ensuring stability regardless of upstream pressure variations, provided the upstream pressure remains above the set point. This functionality is crucial for maintaining desired pressure levels across the network, enhancing system reliability, and preventing damage due to excessive pressure.

The model incorporates a dynamic element through a hydraulic control mechanism, utilizing a feedback loop via a pilot valve to adjust the valve resistance in response to changes in the set point. This dynamic adjustment process, which is captured in the simulation, reflects the pressure-dependent behavior of the PRV as it stabilizes the downstream pressure to the new set point, as described in the following (Prescott and Ulanicki 2003, 2008):

$$\dot{x}_m = \alpha(h_{\text{set}} - h_d) \quad (10)$$

where x_m = new state variable, that represents the percentage of valve opening; h_{set} = PRV set point; and α = valve change rate coefficient, where α can take different values depending on whether the valve is opening or closing, that is

$$\alpha = \begin{cases} \alpha_{\text{open}} & \text{if } h_{\text{set}} > h_d(t-\Delta) \\ \alpha_{\text{closed}} & \text{otherwise} \end{cases} \quad (11)$$

where α_{open} and α_{close} = opening and closing rates of the valve, respectively; and Δ = delay period for the valve mode change operation [$h_d(t-\Delta)$ is used to indicate that α is changed depending on the past value of h_d].

The algebraic component of the model is defined by a conventional valve equation, which can be reformulated as follows:

$$h_u - h_d = \frac{1}{C_v^2}q^2 \quad (12)$$

$$C_v = f(x_m) \quad (13)$$

where C_v = valve's capacity, which is a function of the valve opening. Manufacturers of valves typically provide this relationship, which can be accurately estimated using a second-order polynomial or exponential function. Eq. (12) can be used in place of Eq. (5) for the PRV element in WDS. Following this, the electrical equivalent circuit of PRVs is depicted in Fig. 1(a), demonstrating that PRVs behave as variable resistors. Additionally, it demonstrates how PRVs can be integrated into the EECs of adjacent pipes.

Pump

Pumps are modeled to account for the energy supplied to counteract gravitational and frictional losses, encapsulated by two primary equations. The first, a differential equation, captures pump inertia, and is given by

$$\dot{s} = \frac{1}{T}(v - s) \quad (14)$$

where s = pump speed; v = speed set point; and T = time constant. The second equation, algebraic in nature, quantifies the head increase across the pump as a function of flow rate and pump speed (Ulanicki and Beaujean 2021), and is given by

$$h_d - h_u = k_1 q^2 + k_2 qs + k_3 s^2 \quad (15)$$

where k_1, k_2, and k_3 = empirically determined coefficients.

Pumps in the EEC function analogously to variable voltage sources, and, as demonstrated Fig. 1(b), they can be seamlessly integrated into pipelines. Similar to PRVs, pumps are modeled as two-port elements within the system. Indeed, any dynamic component in the WDS capable of being described by a combination of one algebraic and one ODE can be incorporated into the EWCM as a two-port component. The ODE aspect of these components introduces additional state variables, enriching the flexibility and complexity of the EWC model.

General Structure of an Active Element

From consideration of Eqs. (10) and (14), the general dynamic structure of an active element is given by the linear first order ODE and the algebraic head change equation

$$\frac{dz}{dt} = az + bu$$
$$h_d - h_u = f_e(z, q) \quad (16)$$

where z = elements internal state [$z = s$ for pumps as in Eq. (14)]; and u = control signal (h_{set} for PRVs and v for pumps); a and b = state and input coefficients; and $f_e(z, q)$ = function describing the head change across the element for state z and element flow q [Eq. (12) for PRVs and Eq. (15) for pumps]. For both PRVs and pumps, $b = -a$, and the state equation is of the form

$$\frac{dz}{dt} = a(u - z) \quad (17)$$

which has the interpretation that the state z is drawn to the control u at an exponential rate of a. In the following section, this form of the active element will be incorporated into the network equations for the EWCM.

© ASCE   04025054-3   J. Water Resour. Plann. Manage.

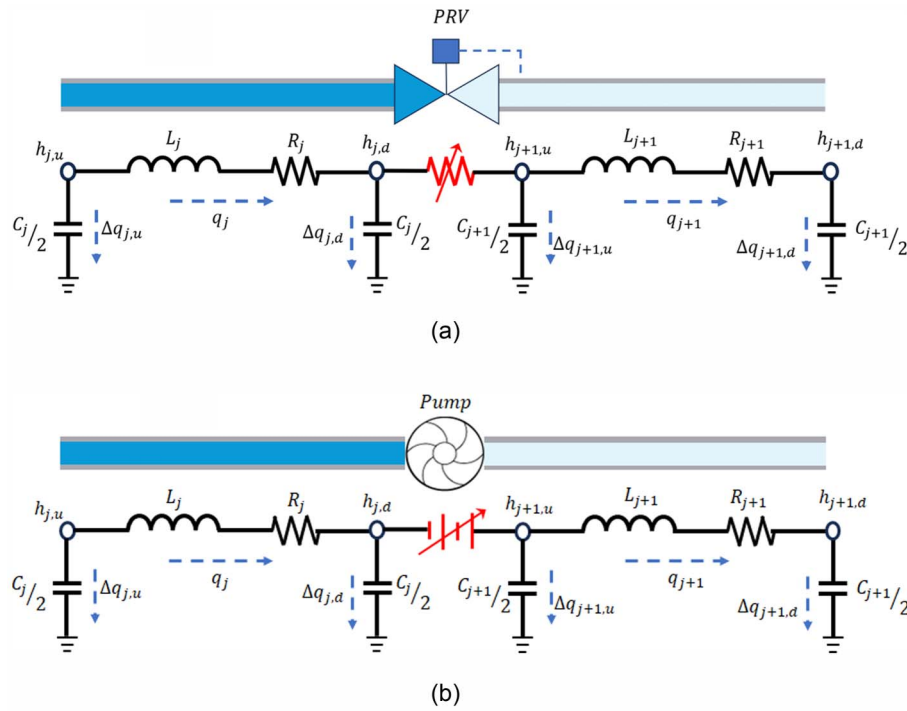J. Water Resour. Plann. Manage., 2025, 151(10): 04025054

Fig. 1. Electrical equivalent circuits for water distribution system components: (a) pipeline configuration featuring two pipes connected by a PRV; and (b) similar pipeline configuration with two pipes and a pump situated in the middle.

Graph-Theoretical Formulation of WDS

For a WDS that includes dynamic elements, the state variables include the hydraulic head at each node (excluding reservoirs), the flow rate in pipes and dynamic elements, and the state variables for the dynamic elements [such as the opening of a PRV, x_m, and pump speed, s, denoted as z in Eq. (15)]. These variables are unknowns, and by determining these variables, the entire state of the system can be identified.

In this paper, PRVs and pumps are considered two-port elements, and the whole system can be represented as a graph of pipes and dynamic elements. Based on graph theory, a graph can be represented by an incidence matrix A, which has a row for each node and a column for each element. The entries of the matrix are either 1, −1, or 0, depending on the relationship between the nodes and edges (for WDS, edges are pipes, PRVs, and pumps). A value of 1 at $A_{i,j}$ indicates that the edge j leaves node i, a value −1 indicates that the edge j enters node i, and value of 0 shows there is no connection between node i and edge j. By having two different types of nodes (internal nodes and reservoir nodes) and two different types of edges (pipes and dynamic elements), the incidence matrix can be divided into different sections as follows:

$$A = \begin{bmatrix} A_I \\ A_R \end{bmatrix}, \qquad A_I = [A_{Ip}|A_{Ie}], \qquad A_R = [A_{Rp}|A_{Re}] \quad (18)$$

where the subscript I = rows associated with internal nodes; R = rows for reservoir nodes; and p and e = pipes and dynamic elements, respectively. Similarly, the vector of nodal heads can be partitioned as follows:

$$h = \begin{bmatrix} h_I \\ h_R \end{bmatrix} \quad (19)$$

where h_I = heads at internal nodes; and h_R = heads at reservoir nodes. Likewise, the vector of link flows can be partitioned as follows:

$$q = \begin{bmatrix} q_p \\ q_e \end{bmatrix} \quad (20)$$

where q_p = flows through pipes; and q_e = flows through dynamic elements.

Based on these partitions, the vector of head differences Δh over each flow element can be written as follows:

$$\Delta h = Ah = \begin{bmatrix} A_I \\ A_R \end{bmatrix}^T \begin{bmatrix} h_I \\ h_R \end{bmatrix} = \begin{bmatrix} A_{Ip}^T & A_{Rp}^T \\ A_{Ie}^T & A_{Re}^T \end{bmatrix} \begin{bmatrix} h_I \\ h_R \end{bmatrix} \quad (21)$$

In this vector, the pressure differences over pipes and dynamic elements have been derived based on the incidence matrix and the vector of nodal pressure heads. Similar to Zeng et al. (2022), the demand vector Q and parameter matrices L, R, C, and T, all of which are diagonal, are utilized in deriving the momentum and continuity equations for pipes. The momentum equation is thereby formulated as follows:

$$L \frac{dq_p}{dt} = -R \text{diag}\{|q_p|\}q_p + A_{Ip}^T h_I + A_{Rp}^T h_R \quad (22)$$

where $|x|$ is the elementwise vector (or matrix) of x, and the continuity equation at nodes can be expressed

$$\left(\frac{1}{2}|A_I|C + T\right)\frac{dh_I}{dt} = A_I q - Q \quad (23)$$

From Eq. (16), the equations for the dynamic elements can be written

$$\frac{dz}{dt} = \text{diag}\{\boldsymbol{a}\}(\boldsymbol{u}_e - \boldsymbol{z})$$

$$\boldsymbol{A}_{Ie}^T \boldsymbol{h}_I + \boldsymbol{A}_{Re}^T \boldsymbol{h}_R - \boldsymbol{F}_e(\boldsymbol{z}, \boldsymbol{q}_e) = 0 \tag{24}$$

where $\boldsymbol{z}$, $\boldsymbol{a}$, and $\boldsymbol{u}_e$ are a vector organization of the states, system coefficients, and control signals for the dynamic elements, respectively; and $\boldsymbol{F}_e(\boldsymbol{z}, \boldsymbol{q}_e)$ = vectorized head change equation for the dynamic elements with states $\boldsymbol{z}$ and element flows $\boldsymbol{q}_e$.

Eqs. (20)–(23), along with Eqs. (11) and (14), form a set of differential algebraic equations (DAEs) for a WDS. In this set of equations, the state vector $\boldsymbol{x}$ can be defined as follows:

$$\boldsymbol{x} = \begin{bmatrix} \boldsymbol{q}_p \\ \boldsymbol{q}_e \\ \boldsymbol{h}_I \\ \boldsymbol{z} \end{bmatrix} \tag{25}$$

and the system inputs are defined

$$\boldsymbol{u} = \begin{bmatrix} \boldsymbol{h}_R \\ \boldsymbol{Q} \\ \boldsymbol{u}_e \end{bmatrix} \tag{26}$$

By applying this state vector to the equations, the nonlinear set of equation can be written as follows:

$$\boldsymbol{E}\dot{\boldsymbol{x}} = f(\boldsymbol{x}, \boldsymbol{u}) \tag{27}$$

where $\boldsymbol{E}$ is a diagonal matrix. Explicitly, this can be given as follows:

$$
\begin{bmatrix} \boldsymbol{I} & 0 & 0 & 0 \\ 0 & 0 & 0 & 0 \\ 0 & 0 & \boldsymbol{I} & 0 \\ 0 & 0 & 0 & \boldsymbol{I} \end{bmatrix} \frac{d}{dt} \begin{bmatrix} \boldsymbol{q}_p \\ \boldsymbol{q}_e \\ \boldsymbol{h}_I \\ \boldsymbol{z} \end{bmatrix} = \begin{bmatrix} 0 & 0 & \boldsymbol{A}_{Ip}^T & 0 \\ 0 & 0 & \boldsymbol{A}_{Ie}^T & 0 \\ \boldsymbol{GA}_{Ip} & \boldsymbol{GA}_{Ie} & 0 & 0 \\ 0 & 0 & 0 & -\boldsymbol{D} \end{bmatrix} \begin{bmatrix} \boldsymbol{q}_p \\ \boldsymbol{q}_e \\ \boldsymbol{h}_I \\ \boldsymbol{z} \end{bmatrix}
$$
$$
- \begin{bmatrix} \boldsymbol{F}_p(\boldsymbol{q}_p) \\ \boldsymbol{F}_e(\boldsymbol{z}, \boldsymbol{q}_e) \\ 0 \\ 0 \end{bmatrix} + \begin{bmatrix} \boldsymbol{A}_{Rp}^T & 0 & 0 \\ \boldsymbol{A}_{Re}^T & 0 & 0 \\ 0 & -\boldsymbol{G} & 0 \\ 0 & 0 & \boldsymbol{D} \end{bmatrix}
$$
$$
\times \begin{bmatrix} \boldsymbol{h}_R \\ \boldsymbol{Q} \\ \boldsymbol{u}_e \end{bmatrix} \tag{28}
$$

where

$$\boldsymbol{D} = \text{diag}\{\boldsymbol{a}\} \boldsymbol{G} = \left(\frac{1}{2}|\boldsymbol{A}_I|\boldsymbol{C} + \boldsymbol{T}\right)^{-1} \boldsymbol{F}_p(\boldsymbol{q}_p) = \boldsymbol{L}^{-1}\boldsymbol{R}\text{diag}\{|\boldsymbol{q}_p|\}\boldsymbol{q}_p$$

This set of equations is in a nonlinear state-space format and can be integrated using various numerical integration techniques, such as ode15s or ode23t in MATLAB version R2023a, which are suitable for DAEs. The matrix G contains the capacitance terms, which are directly related to the compressibility of water and its ability to store energy during transient events. The function $\boldsymbol{F}_p(\boldsymbol{q}_p)$ accounts for nonlinear damping effects, influencing how transient waves dissipate over time due to friction. The matrix D contains the time constant values for PRVs and pumps, which dictate the dynamic response of these elements within the system. An important advantage

of this state-space representation is its ability to facilitate various control analyses, including stability, observability, and modal analysis of WDS. To enhance the accuracy of EWCM pipes, they can be discretized into multiple elements. Discretization alters the structure of matrices, such as A_I, and affects the size of other vectors. A detailed explanation of how to discretize each pipe and create a new system of equations from Eq. (28) has been provided by Zeng et al. (2022).

Numerical Simulation

In this section, the EWCM was first verified against the MOC and RWCM under slow transient conditions, demonstrating that the EWCM accurately replicates system behavior in these scenarios. Subsequently, two fast transient tests were conducted to further evaluate the EWCM's performance. The results highlight that, even under faster transient conditions, the EWCM maintained accuracy, particularly when the number of reaches was appropriately increased.

Case Study 1: Numerical Verification

The objective of this verification study was to validate the EWCM with dynamic elements using an established test case from Prescott and Ulanicki (2003), demonstrated in Fig. 2(a). Additionally, the test case was also simulated using RWCM and MOC for comparison. The spatial step for the MOC simulation has been chosen to be 0.1 m for each pipe. The setup includes two valves located at the upstream and downstream ends of a PRV. Two transient events were simulated:
- Increasing the set point of the PRV: Between 18 and 20 s, the set point of the PRV was altered from 32.6 to 36.6 m.
- Partial closure of upstream valve: Between 64 and 66 s, the upstream valve opening was adjusted, and the minor loss coefficient (Kv) was changed from 46 to 83.

The results obtained from the EWCM, RWCM, and MOC were compared as illustrated in Fig. 3. The comparison shows that an increase in the PRV set point caused the valve to open further, maintaining a constant downstream head and increasing flow. This flow stabilized in approximately 15 s, with the duration depending on the α parameter. When the upstream valve was closed, the flow decreased, causing a drop in pressure both upstream and downstream of the PRV. To compensate, the PRV opened more significantly, restoring the flow. Eventually, the flow returned to its original level as the pressure drop across the upstream valve was balanced by a decrease in the pressure drop across the PRV.

The comparison between the models shows that the EWCM and RWCM performed similarly to the MOC in slow transient scenarios. Therefore, it can be concluded that for slow transients, all models exhibited comparable performance. However, further comparisons under fast transient conditions are necessary to fully assess the models' effectiveness.

Case Study 2: Fast Transient Comparison

In order to clearly discern the differences between these models, two fast transient scenarios were simulated. This was achieved by using a configuration similar to the previous section, but with altered pipe lengths, diameters, and modified PRV parameters. Increasing the length and diameter of the pipes makes water compressibility more significant. Consequently, a valve closure time of less than 4 s constitutes a fast transient in this new configuration, making the distinctions between these models more apparent. The new parameters for the setup are shown in Fig. 3(b). The spatial
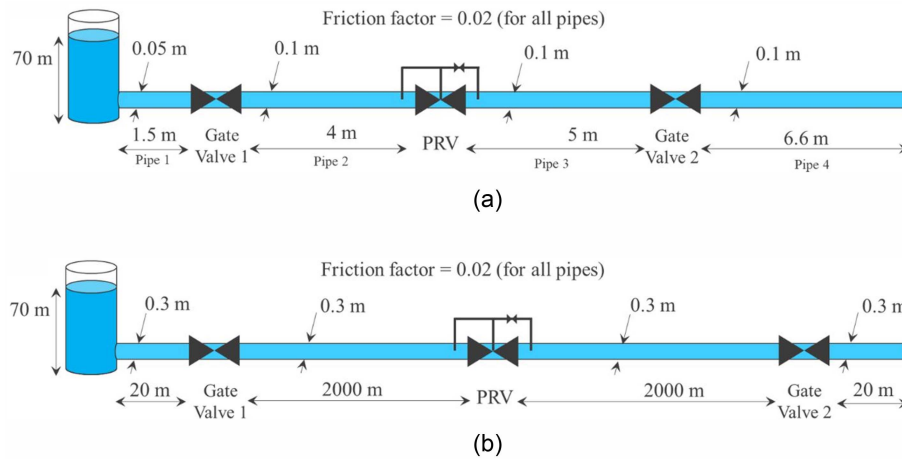
© ASCE   04025054-5   J. Water Resour. Plann. Manage.

J. Water Resour. Plann. Manage., 2025, 151(10): 04025054

Fig. 2. Pipeline configuration for (a) slow transient analysis, based on experimental setup by Prescott and Ulanicki (2003); and (b) fast transient analysis (Case studies 2 and 3).

step for the MOC simulation has been chosen to be 10 m for each pipe.

In this test, the upstream valve closure was altered from $Kv = 50$ to 400 in two different scenarios. In Scenario 1, the valve closure duration was 2 s, whereas in Scenario 2, the valve closure duration was 1 s. The Kv increased during these two scenarios with a cosine pattern.

First, the simulation results for Scenario 1 will be presented. Fig. 4 displays the flow through the PRV. Like the slow transient scenario, the flow reached the same level after the transient event. The MOC was considered the baseline for accuracy, and the other models were compared against it. To assess the similarity of these models to the MOC results, the normalized root-mean square deviation (NRMSD) was calculated as follows and is reported for each model in the figure:

$$\text{NRMSD} = \frac{\sqrt{\sum_{i=1}^{N} (\hat{x}_i - x_i)/N}}{(x_{\max} - x_{\min})} \times 100 \qquad (29)$$

where $\hat{x}_i$ = results obtained from the MOC; and x_i = results from the other models. It was observed that increasing the number of elements, particularly for the two longest pipes, enhanced the accuracy of the EWCM.

Figs. 5(a and b) illustrate the pressure variations upstream and downstream of the PRV for Scenario 1. The number of reaches in Fig. 6 represents the number of segments for Pipes 2 and 3. These figures reveal that the NRMSE was higher for the RWCM and suggest that this error can be reduced by increasing the number of reaches in the EWCM for pipes. To emphasize the differences between these models, the pressure results immediately after the PRV are zoomed in and depicted in Fig. 5(b). In the RWCM, the primary assumption was that of an infinite wave speed. Due to this assumption, an immediate pressure change was observed following the closure of the upstream valve, which is not realistic. In contrast, the MOC indicates a 2-s delay for the wave to reach the PRV, which aligns with the expected time duration for a wave to travel that distance (given a 2,000 m length for Pipe 2 and a wave speed of 1,000 m/s).

The EWCM could capture this delay even with only one element per pipe, and its accuracy improved with an increased number of elements. The error in the delay duration doubled for the second wave, and this trend continued for subsequent waves if only one element was used. Moreover, the wave shape became more closely

aligned with the actual scenario when the EWCM had more elements. The MOC depicted a sharp wave for this transient event, and the EWCM with 10 elements could capture these wave shapes, demonstrating its effectiveness in simulating fast transient events. Zeng et al. (2022) showed that if the bandwidth of the transient generated at the boundary conditions is lower than the critical frequency ($f_c = a/10l$), the EWCM matched the accuracy of the MOC. However, discrepancies increased when the system was excited with higher frequency bandwidths. The critical frequency and the excitation frequency bandwidth can be used to determine the number of elements for each pipe when high accuracy is required. However, as shown in Fig. 6, the EWCM, even with a single element still performed better than the RWCM.

Fig. 6 represents the PRV's opening as a percentage over time. The influence of the hydraulic controller of the PRV, implicit in the α parameters, moderated the rate of PRV opening changes, resulting in remarkably similar outcomes across the three models. However, an exception was observed in the RWCM, where the anticipated delay at the onset of the opening change was absent.

Next, by simulating Scenario 2 with a faster valve closure, Fig. 7 illustrates the pressure variations upstream and downstream of the PRV, along with the NRMSE reported in the figure. In this scenario, the valve closure was faster, and the NRMSE of the EWCM increased compared with Scenario 1. Although this transient is fast, the EWCM with only 10 reaches still showed relatively small error. As seen from the comparison of the two scenarios, as the transient became faster, the number of reaches had to be increased to maintain a fixed amount of error.

Numerical Considerations

In this section, two key numerical aspects of the EWCM were investigated. First, the stiffness of the ODE-based models, EWCM and RWCM, was measured and compared. Second, the sparsity of the EWCM was examined in relation to its effect on computational efficiency because it reduces matrix operation complexity, particularly in large-scale water distribution systems.

Stiffness

In this section, the focus is on comparing the inherent stiffness of the EWCM and RWCM, both of which are ODE-based method.
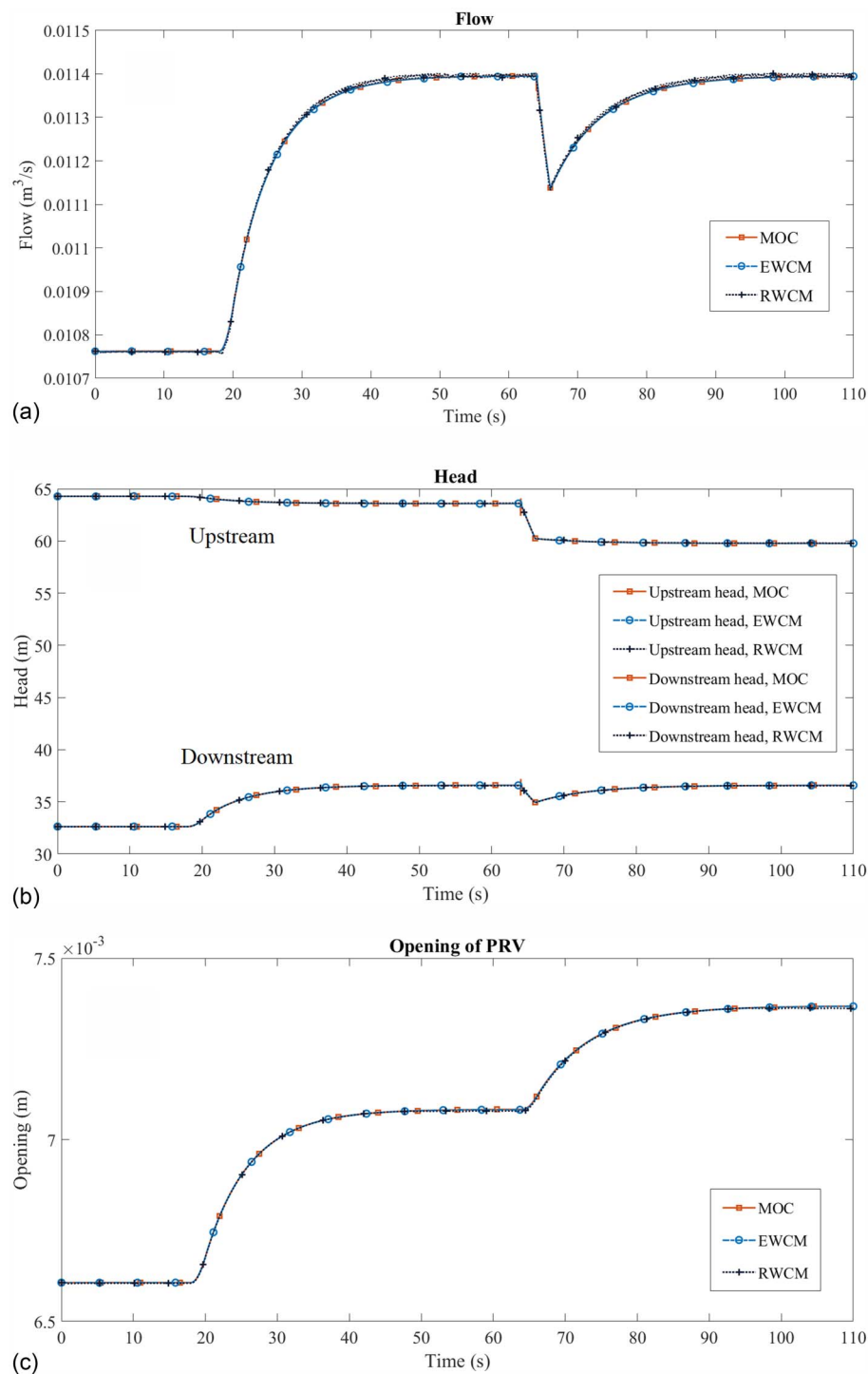
Fig. 3. Simulation results from MOC, EWCM, and RWCM: (a) flow through the PRV; (b) upstream and downstream head of the PRV; and (c) opening of the PRV.

Stiffness refers to the presence of rapidly varying solution components alongside slowly varying ones, which can significantly affect the stability and accuracy of numerical integration. In the context of ODE-based methods for transient analysis, stiffness arises due to the wide range of time scales associated with wave propagation in the system (Hairer and Wanner 1996). Stiffness can significantly affect the stability and accuracy of the numerical integration process. The stiffness is quantified by the ratio of the largest to the smallest eigenvalue of the system, derived from the Jacobian matrix of each model.

Case Study 1: Pipe Network
The EWCM defines the system state by considering both the head at the nodes and the flow in the pipes, whereas the RWCM, following Shimada (1992), considers only the independent pipe flows as the system state. This results in differing structures for their Jacobian matrices, with the EWCM's matrix being notably simpler to compute, as detailed in the Appendix I. The Jacobian matrix can also be determined using the Simulink environment in MATLAB. In this approach, the equations are first converted into a Simulink model, and then the 'linearize' function or the Model Linearizer App
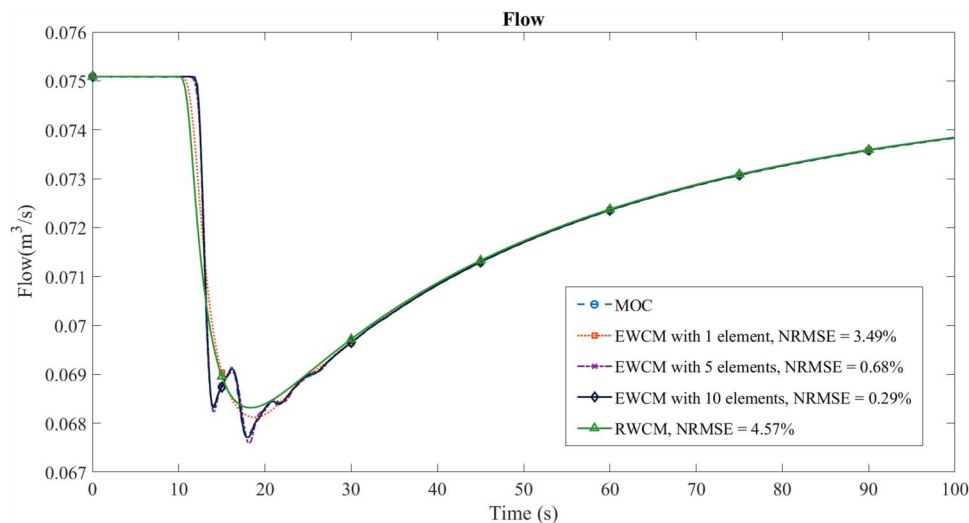
© ASCE 04025054-7 J. Water Resour. Plann. Manage.

J. Water Resour. Plann. Manage., 2025, 151(10): 04025054

Fig. 4. Flow through the PRV for fast transient event (Scenario 1).
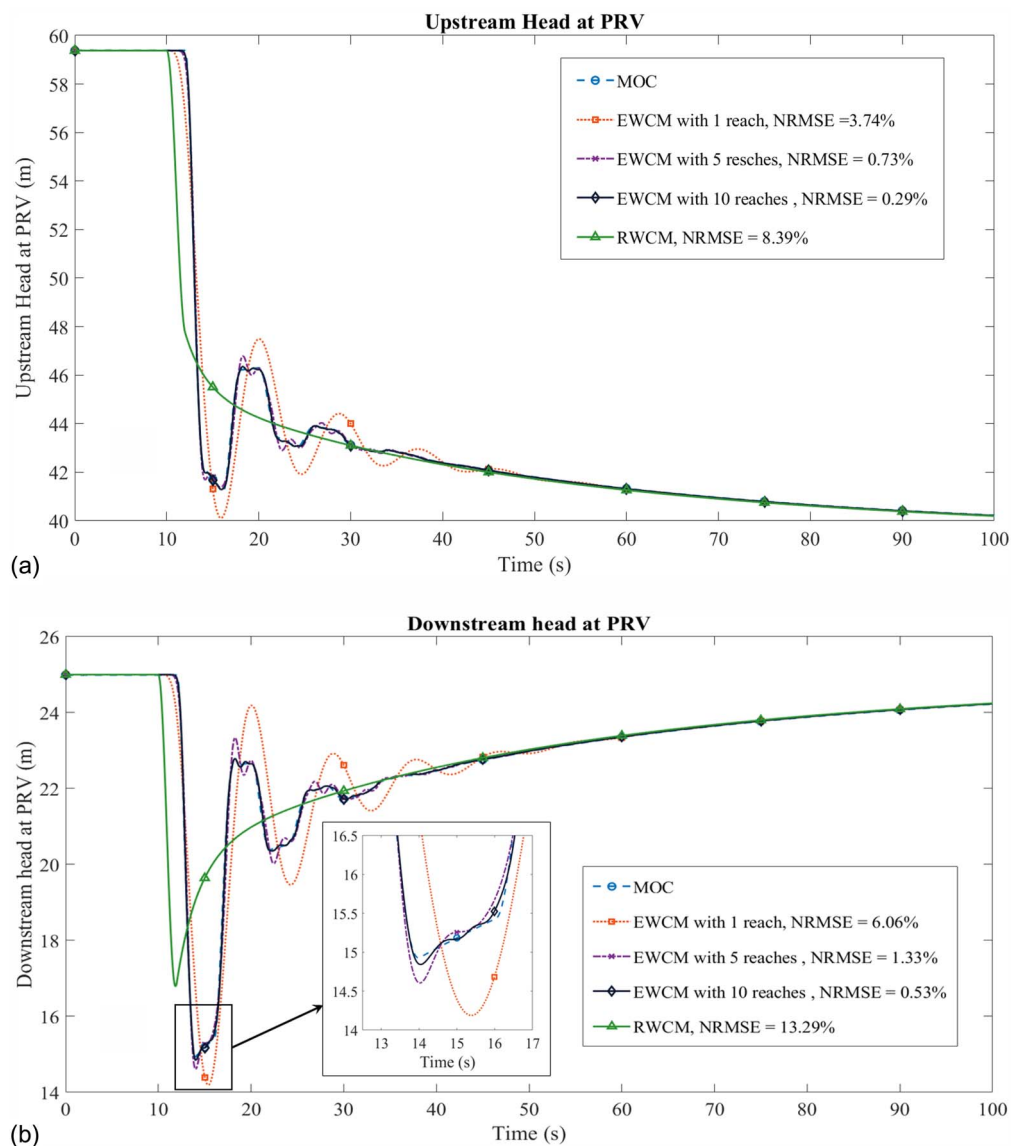

Fig. 5. Simulation results from MOC, EWCM with 1, 5, and 10 elements, and RWCM for Scenario 1: (a) pressure head upstream of the PRV; and (b) pressure head downstream of the PRV.
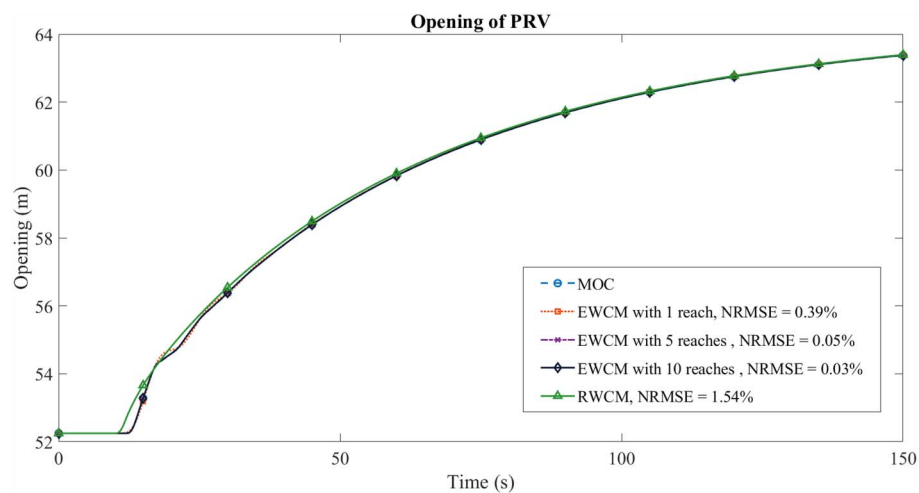
© ASCE 04025054-8 J. Water Resour. Plann. Manage.

J. Water Resour. Plann. Manage., 2025, 151(10): 04025054
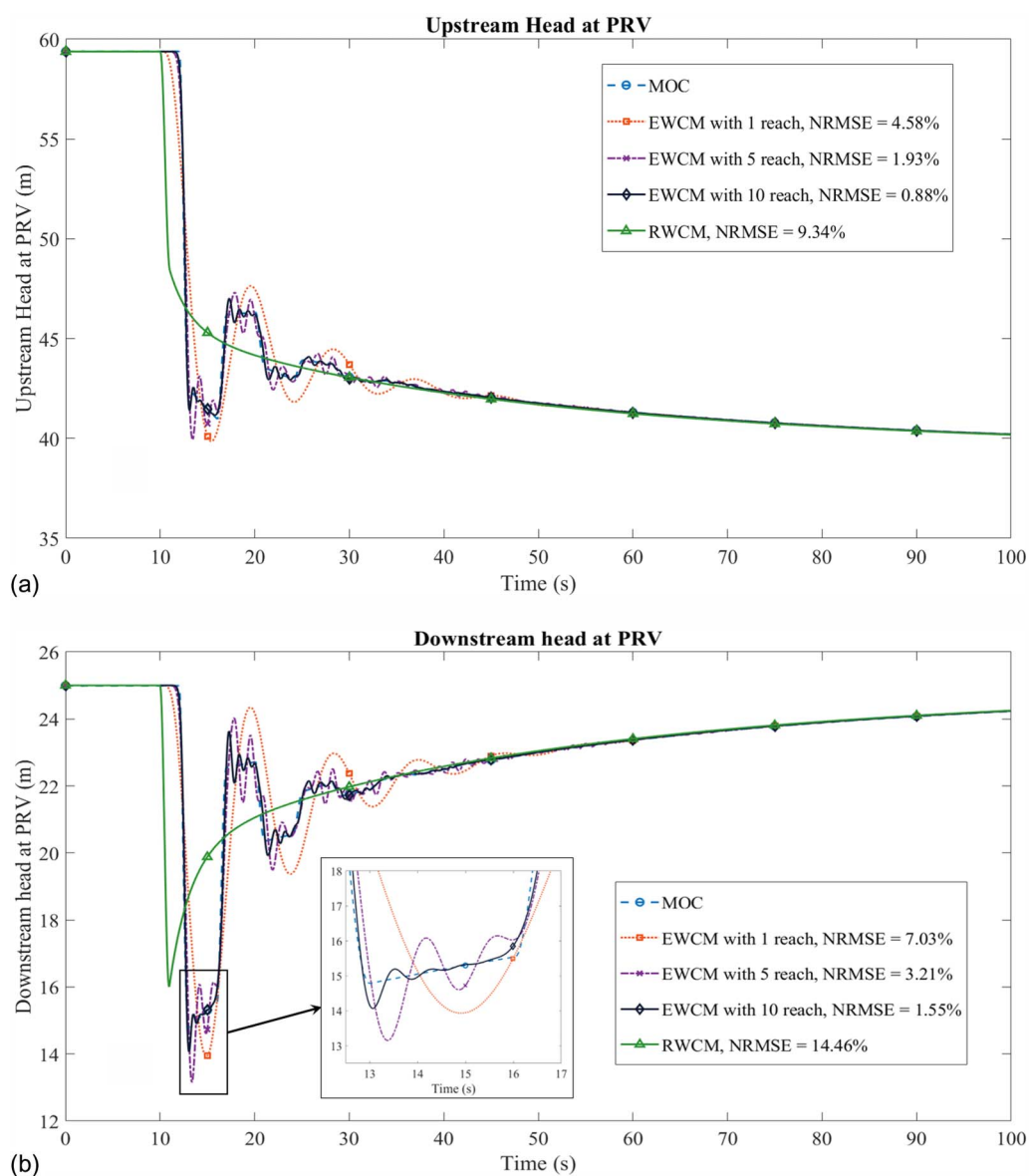
Fig. 6. Opening of the PRV.

Fig. 7. Simulation results from MOC, EWCM with 1, 5, and 10 elements and RWCM for scenario 2: (a) upstream pressure head at the PRV; and (b) downstream pressure head at the PRV.
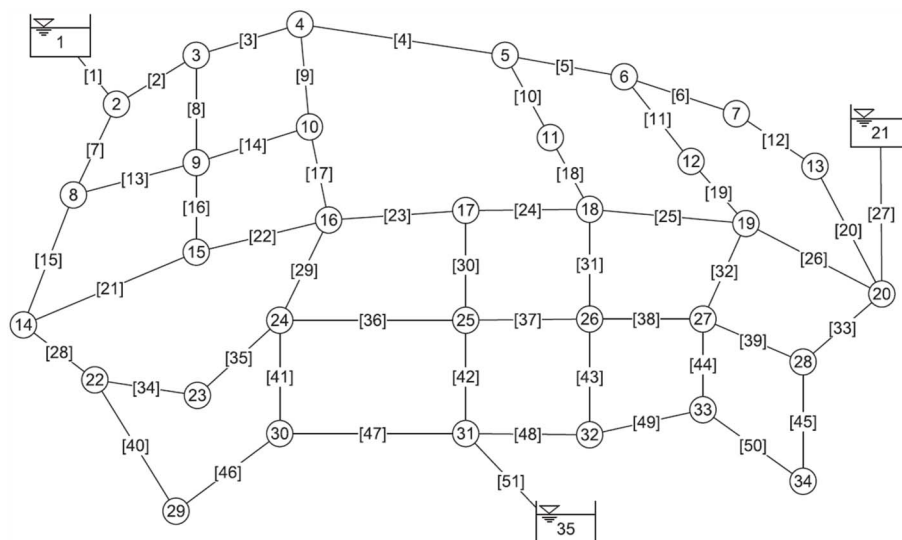
© ASCE 04025054-9 J. Water Resour. Plann. Manage.

J. Water Resour. Plann. Manage., 2025, 151(10): 04025054

Fig. 8. Pipe network featuring three reservoirs, comprising 51 edges and 32 internal nodes, as detailed by Zecchin (2010).

in Simulink is used to derive a linear state space model of the system around an operating point. MATLAB calculates the Jacobian of the system by numerically perturbing the variables and measuring the slope of the changes. Both of these methods have been used for finding the Jacobian matrix in this section.

To examine the intrinsic characteristics of these models, a 51-pipe network was analyzed, as detailed in Fig. 8. In this network, the only components are pipes, making the system of equations solely ODEs. This setup is appropriate for comparing the stiffness of the EWCM and RWCM. This specific network configuration has previously been utilized for the study of hydraulic transients by Vítkovský (2001) and Zecchin (2010). It was presumed that the wave speed across all pipes was 1,000 m/s. Although this paper does not elaborate on the network's intricate details due to space constraints, it encompasses a variety of network parameters, including pipe lengths ranging from 450 to 994 m, diameters from 304.8 to 1,524 mm, and nodal demands up to 0.280 L/s. Further details on the case study have been given by Zecchin (2010).

A transient event was simulated, involving a reduction in demand at each node by half over a 10-s period from 10 to 20 s.

The stiffness metrics for the EWCM and RWCM over time are presented in Figs. 9 and 10.

The results indicate higher stiffness in the EWCM. Although stiffness allows the model to capture a wider range of frequencies, it also introduces numerical challenges. Stiff systems require solvers capable of handling rapidly changing dynamics to maintain stability and accuracy. In MATLAB, explicit solvers like ode45, which use Runge–Kutta methods, may struggle with stiff systems and lead to numerical instability or excessive computation time. Instead, solvers designed for stiff problems, such as ode15s, may be more appropriate, depending on the severity of the stiffness. If a simulation encounters instability or crashes, switching to a stiff solver is necessary to ensure reliable results. Although this complexity increases the computational effort and solver selection becomes more critical, it allows for a more accurate representation of system dynamics.

Case Study 2: Pipe Network with PRV

To extend the analysis and comparison of the stiffness of the EWCM and RWCM for systems having PRVs, Case study 2 from the "Numerical Simulation" section has been used. The same
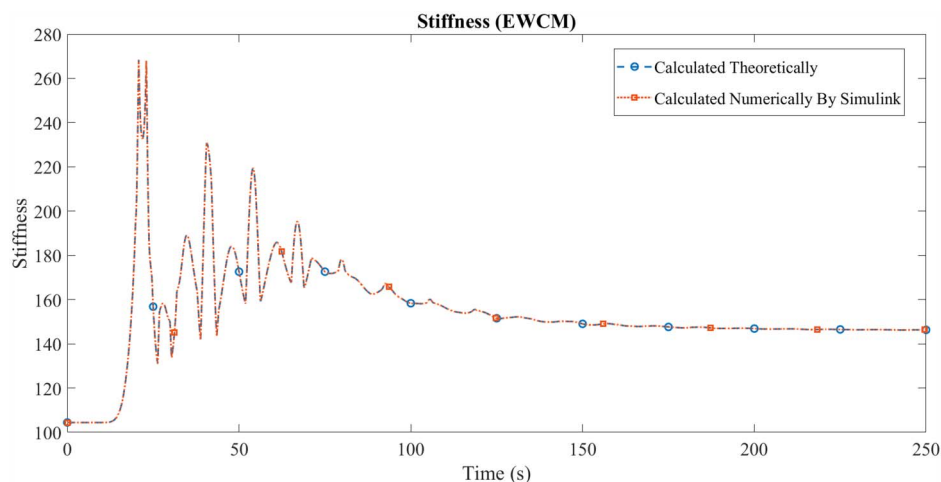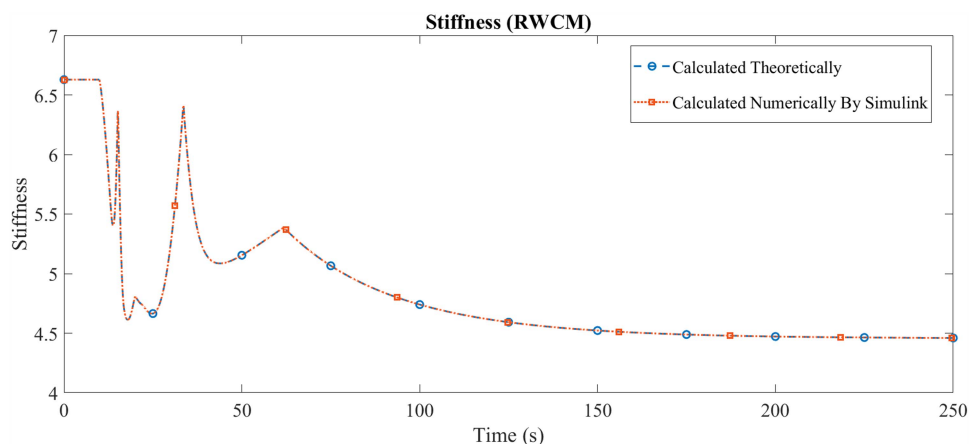

Fig. 9. Stiffness of EWCM.
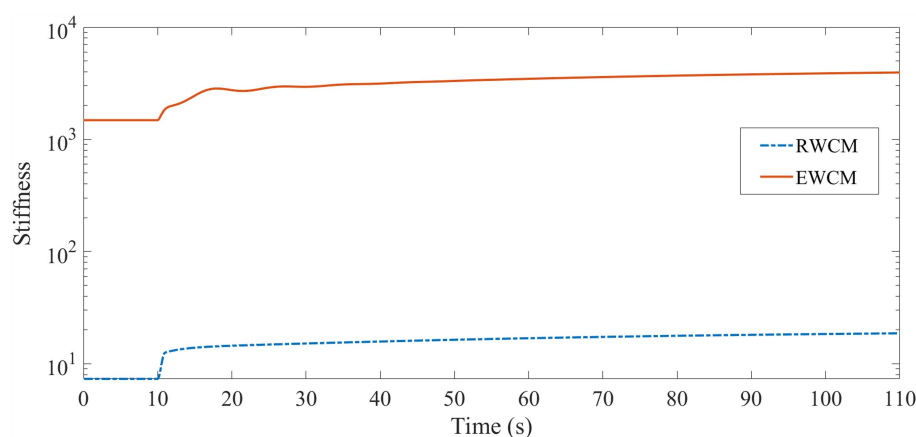
Fig. 10. Stiffness of RWCM.

Fig. 11. Stiffness of RWCM for Case study 2.

transient event was utilized, and the stiffness for both models was calculated using Simulink software. The results are shown in Fig. 11. Because a PRV is present in the pipeline, the system of equations would be DAEs. As can be seen, the EWCM was even stiffer than the RWCM in Case study 2, which includes a PRV, compared with Case study 1 where the system comprised only pipes.

Sparsity

Building upon the findings from the previous sections, it is evident that the EWCM handles fast transient events in WDS with improved accuracy when more elements are used per pipe. A closer examination of its matrix formulation reveals that key matrices, such as A_I and A_R, are sparse, particularly for large systems. Sparsity in this context means that the matrices contain a high proportion of zero values, reducing the memory footprint and computational overhead (da Silva Lessa et al. 2020). These matrices can be converted into sparse matrices with prebuilt function like *sparse* in MATLAB for simulations. Using sparse matrices reduces memory usage and computational time, as demonstrated in the 51-pipe network simulation over 400 s with varying elements per pipe. Fig. 12 illustrates the computation time, and Fig. 13 depicts the memory usage for both regular and sparse matrix implementations.

As the number of elements increased, computation time and memory usage rose exponentially. However, using sparse matrices mitigated this increase, which can be beneficial for large-scale systems. The extent of this improvement may vary depending on the specific case, as computational efficiency is influenced by factors such as network configuration, solver selection, and hardware specifications. Nevertheless, the results indicate that implementing EWCM with a sparse matrix structure generally led to improved efficiency. By running the same test case with the same time step and a spatial step of 10 m for each pipe, the MOC simulation took 288 s, which is higher than both RWCM (1.5 s) and EWCM. In contrast to the MOC, which is computationally demanding, the EWCM offers reasonable accuracy for fast transient events in large-scale networks within a reduced time frame. This efficiency makes the EWCM particularly advantageous for optimization and control applications in WDS.

Conclusion

This study introduced the integration of dynamic elements into the EWCM through electrical equivalent circuits for PRVs and pumps, benchmarking its effectiveness against existing results. It compares the EWCM with the RWCM and MOC across slow
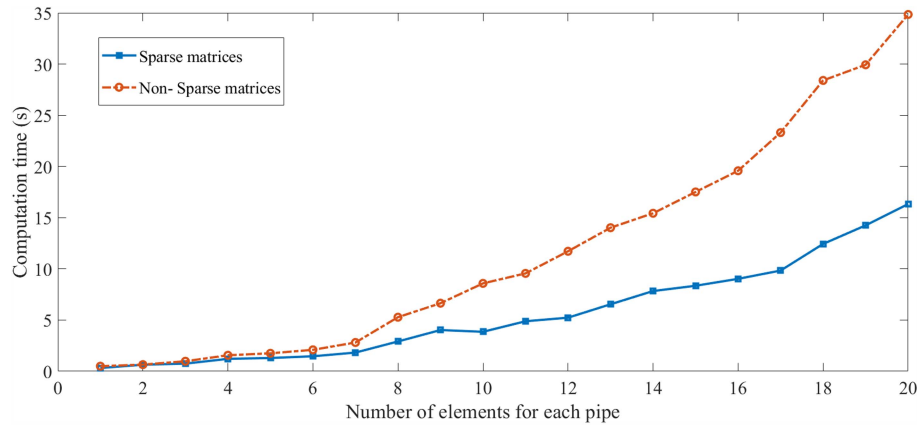
© ASCE 04025054-11 J. Water Resour. Plann. Manage.

J. Water Resour. Plann. Manage., 2025, 151(10): 04025054
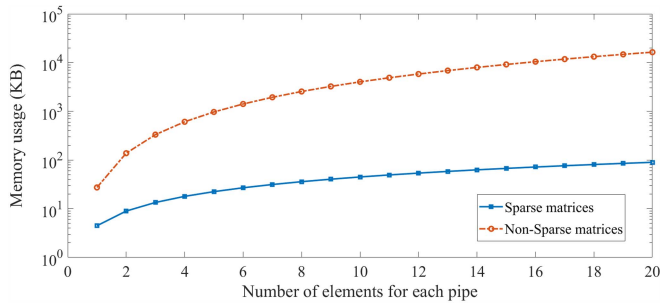
Fig. 12. Computation time.

Fig. 13. Memory usage.

and fast transient events in water distribution systems. The results showed that the EWCM performs comparably to other models during slow transient scenarios and provides a useful approximation during fast transient events.

Comparative analysis suggested that the EWCM can achieve accuracy comparable to the MOC in fast transient scenarios. Furthermore, this accuracy can be enhanced by increasing the level of discretization, albeit at some cost to the required computational time. This flexibility allows for a tailored balance between accuracy and computational efficiency, a feature not available with the RWCM. Thus, the EWCM offers a unique advantage in water distribution system analysis by allowing users to adjust its performance according to their specific needs for accuracy and computational resources.

The EWCM was also identified as being stiffer than the RWCM. Although this stiffness allows for representing dynamic events across a broad frequency range, it also increases complexity in numerical integration. The study highlighted the role of sparse matrices within the EWCM, which can improve computational efficiency in large-scale networks by reducing computation time and memory usage. The combination of stiffness and sparsity provides a framework for analyzing large networks, which may be useful in optimization and control strategies within WDS, depending on the specific requirements of an application.

Appendix I. Jacobian Matrix for EWCM

For a WDS lacking dynamic components, the EWCM system of equations is outlined as follows:

$$
\left\{ \begin{array}{c} \dfrac{d\boldsymbol{q}}{dt} \\ \dfrac{d\boldsymbol{h}_I}{dt} \end{array} \right\} = \left\{ \begin{array}{c} \boldsymbol{L}^{-1}(-\boldsymbol{R}\mathrm{diag}\{|q|\}q + \boldsymbol{A}_I^T\boldsymbol{h}_I + \boldsymbol{A}_R^T\boldsymbol{h}_R) \\ \left(\mathrm{diag}\left(\dfrac{1}{2}|\boldsymbol{A}_I|\boldsymbol{C} + \boldsymbol{T}\right)\right)^{-1}(\boldsymbol{A}_I\boldsymbol{q} - \boldsymbol{Q}_I) \end{array} \right\} \tag{30}
$$

In this system, the state variables are $\boldsymbol{q}$ and $\boldsymbol{h}_I$. By taking the derivative, the structure of the Jacobian matrix can be obtained. The size of this matrix is 83×83 ($83 = 51$ edges $+ 32$ internal nodes) for a 51-pipe network. In this structure, the bottom-right portion of the matrix consists entirely of zeros, and the top-left portion is diagonal. The top-right and bottom-left portions contain nonzero elements depending on the network's structure. However, in a large network, most elements in these two parts are also zero.

Appendix II. Jacobian Matrix for RWCM

In the RWCM, the model utilizes fewer state variables compared with the EWCM. Specifically, the state variables in RWCM are confined to the independent flow variables. For instance, in a network consisting of 51 pipes, there are only 19 independent flows, which can be obtained from the calculation of 51 edges minus 32 internal nodes. This reduction in state variables complicates the process of deriving the Jacobian matrix from the momentum equation because the limited and interconnected state variables pose challenges.

The fundamental equations for RWCM, which assume infinite wave speed (a key assumption of this method), are outlined as follows:

$$
\boldsymbol{L}\frac{d\boldsymbol{q}}{dt} = -\boldsymbol{R}|\boldsymbol{q}|\boldsymbol{q} + \boldsymbol{A}_I^T\boldsymbol{h}_I + \boldsymbol{A}_R^T\boldsymbol{h}_R \tag{31}
$$

$$
\boldsymbol{A}_I\boldsymbol{q} = -\boldsymbol{Q}_I \tag{32}
$$

Derivation begins by differentiating Eq. (32) and substituting Eq (31) into it, yielding the following expression for $\boldsymbol{h}_I$:

$$
\boldsymbol{h}_I = \boldsymbol{K}^{-1}\left[-\frac{\boldsymbol{Q}_I(t)}{dt} - \boldsymbol{A}_I\boldsymbol{L}^{-1}[-\boldsymbol{R}q|q| + \boldsymbol{A}_R^T\boldsymbol{h}_R] \right] \tag{33}
$$

where $\boldsymbol{K} = \boldsymbol{A}_I\boldsymbol{L}^{-1}\boldsymbol{A}_I^T$. Subsequently, when $\boldsymbol{h}_I$ is substituted back into Eq. (31), the following expression is derived:

$$\frac{\partial \boldsymbol{q}}{\partial t} = \boldsymbol{L}^{-1}\{-\boldsymbol{R}\boldsymbol{q}|\boldsymbol{q}| + \boldsymbol{A}_I^T \boldsymbol{K}^{-1}\boldsymbol{A}_I \boldsymbol{L}^{-1}\boldsymbol{R}\boldsymbol{q}|\boldsymbol{q}|\}$$
$$+ \boldsymbol{L}^{-1}\boldsymbol{A}_I^T\left\{(\boldsymbol{K})^{-1}\left[-\frac{\boldsymbol{Q}_I(t)}{dt}\right]\right\}$$
$$+ \boldsymbol{L}^{-1}\{-\boldsymbol{A}_I^T \boldsymbol{K}^{-1}\boldsymbol{A}_I \boldsymbol{L}^{-1}\boldsymbol{A}_R^T \boldsymbol{h}_R + \boldsymbol{A}_R^T \boldsymbol{h}_R\} \quad (34)$$

By defining $\boldsymbol{W} = \boldsymbol{L}^{-1}(\boldsymbol{I} - \boldsymbol{A}_I^T \boldsymbol{K}^{-1}\boldsymbol{A}_I \boldsymbol{L}^{-1})$ and incorporating the permutation matrix $\boldsymbol{P}$, which is used to order the state variables based on independent and dependent flows, the following refined equation is obtained:

$$\boldsymbol{P}\frac{d\boldsymbol{q}}{dt} = \boldsymbol{P}\boldsymbol{W}\boldsymbol{P}^{-1}\boldsymbol{P}[-\boldsymbol{R}\boldsymbol{q}|\boldsymbol{q}| + \boldsymbol{A}_R^T \boldsymbol{h}_R] + \boldsymbol{P}\boldsymbol{L}^{-1}\boldsymbol{A}_I^T \boldsymbol{K}^{-1}\frac{d\boldsymbol{Q}_I}{dt} \quad (35)$$

The first n_i rows of this equation set form a set of ODEs for RWCM, from which $\boldsymbol{q}_i$ (the independent flow rates) can be determined. Through Eq. (35), the matrix expression is simplified, and Eq. (25) details the dynamic of $\boldsymbol{q}_i$

$$\boldsymbol{P}\boldsymbol{W}\boldsymbol{P}^{-1} = \begin{pmatrix} \boldsymbol{W}_i \\ \boldsymbol{W}_d \end{pmatrix} \quad (36)$$

$$\frac{d\boldsymbol{q}_i}{dt} = \boldsymbol{W}_i\boldsymbol{P}[-\boldsymbol{R}\boldsymbol{q}|\boldsymbol{q}| + \boldsymbol{A}_R^T \boldsymbol{h}_R] + \boldsymbol{P}\boldsymbol{L}^{-1}\boldsymbol{A}_I^T \boldsymbol{R}^{-1}\frac{d\boldsymbol{Q}_I}{dt} \quad (37)$$

On the other hand, the flow vector $\boldsymbol{q}$ is divided into $\boldsymbol{q}_i$ and $\boldsymbol{q}_d$ (dependent flow rates), with $\boldsymbol{q}_d$ being expressed as a function of $\boldsymbol{q}_i$ as per Shimada (1992) as follows:

$$\boldsymbol{q}_d = -\boldsymbol{A}_{Id}^{-1}(\boldsymbol{A}_{Ii}\boldsymbol{q}_i + \boldsymbol{Q}_I) \quad (38)$$

Two additional matrices, $\boldsymbol{E}_{i1}^T$ and $\boldsymbol{E}_{i2}^T$, are defined for the decomposition of $\boldsymbol{W}_i$ as follows:

$$\boldsymbol{E}_{i1}^T = [\boldsymbol{I}_{ni} \quad \boldsymbol{0}_{n_i \times n_D}] \quad (39)$$

$$\boldsymbol{E}_{i2}^T = [\boldsymbol{0}_{n_D \times n_i} \quad \boldsymbol{I}_{n_D}] \quad (40)$$

where n_D = number of dependent pipes; and n_i = number of independent pipes. By applying Eqs. (39) and (40), on the first term of the right-hand side of Eq. (37), the following relationship is established

$$\boldsymbol{W}_i\boldsymbol{P}[-\boldsymbol{R}\boldsymbol{q}|\boldsymbol{q}|] = \boldsymbol{W}_{i1}(-\boldsymbol{R}|\boldsymbol{q}_i|)\boldsymbol{q}_i + \boldsymbol{W}_{i1}(-\boldsymbol{R}|\boldsymbol{q}_d|)\boldsymbol{q}_d \quad (41)$$

$$\begin{aligned} \boldsymbol{W}_{i1} &= \boldsymbol{W}_i\boldsymbol{E}_{i1}^T \\ \boldsymbol{W}_{i2} &= \boldsymbol{W}_i\boldsymbol{E}_{i2}^T \end{aligned} \quad (42)$$

Eq. (38) is substituted into Eq. (41), resulting in

$$\boldsymbol{W}_i\boldsymbol{P}[-\boldsymbol{R}\boldsymbol{q}|\boldsymbol{q}|] = \boldsymbol{W}_{i1}(-\boldsymbol{R}|\boldsymbol{q}_i|)\boldsymbol{q}_i$$
$$+ \boldsymbol{W}_{i2}(-\boldsymbol{R}|\boldsymbol{q}_d|)(-\boldsymbol{A}_{Id}^{-1}(\boldsymbol{A}_{Ii}\boldsymbol{q}_i + \boldsymbol{Q}_I)) \quad (43)$$

With Eq. (43) substituted into Eq. (37) and upon taking the derivative, the Jacobian matrix is derived as follows:

$$\boldsymbol{J} = -2\boldsymbol{W}_{i1}\mathrm{diag}(\boldsymbol{R}_i|\boldsymbol{q}_i|)$$
$$- 2\boldsymbol{W}_{i2}\mathrm{diag}(\boldsymbol{R}_d| - \boldsymbol{A}_{Id}^{-1}(\boldsymbol{A}_{Ii}\boldsymbol{q}_i + \boldsymbol{Q}_I)|)(-\boldsymbol{A}_{Id}^{-1}(\boldsymbol{A}_{Ii})) \quad (44)$$

Data Availability Statement

Some or all data, models, or code that support the findings of this study are available from the corresponding author upon reasonable request.

Author Contributions

Morteza Imani: Conceptualization; Formal analysis; Investigation; Validation; Visualization; Writing – original draft. Aaron Zecchin: Conceptualization; Funding acquisition; Project administration; Supervision; Writing – original draft; Writing – review and editing. Wei Zeng: Conceptualization; Funding acquisition; Investigation; Resources; Supervision; Writing – review and editing. Martin F. Lambert: Conceptualization; Funding acquisition; Supervision; Writing – review and editing.

References

Creaco, E., A. Campisano, M. Franchini, and C. Modica. 2017a. "Unsteady flow modeling of pressure real-time control in water distribution networks." *J. Water Resour. Plann. Manage.* 143 (9): 04017056. https://doi.org/10.1061/(ASCE)WR.1943-5452.0000821.

Creaco, E., G. Pezzinga, and D. Savic. 2017b. "On the choice of the demand and hydraulic modeling approach to WDN real-time simulation." *Water Resour. Res.* 53 (7): 6159–6177. https://doi.org/10.1002/2016WR020104.

da Silva Lessa, L., C. C. S. de Luca, T. G. Pereira, C. V. C. Grilo, A. C. Moreira, C. M. B. Ronchini, E. M. Gennaro, P. G. Der Agopian, and A. J. do Prado. 2020. "Sparse matrices for transient simulations with computing memory reduction." *Electr. Power Syst. Res.* 183 (Jun): 106266. https://doi.org/10.1016/j.epsr.2020.106266.

Hairer, E., and G. Wanner. 1996. *Solving ordinary differential equations II: Stiff and differential-algebraic problems*. Berlin: Springer.

Jaeger, C. 1977. *Fluid transients in hydro-electric engineering practice*. Glasgow, Scotland: Blackie.

Khilqa, S., M. Elkholy, M. Al-Tofan, J. M. Caicedo, and M. H. Chaudhry. 2019. "Uncertainty quantification for damping in transient pressure oscillations." *J. Water Resour. Plann. Manage.* 145 (9): 04019039. https://doi.org/10.1061/(ASCE)WR.1943-5452.0001089.

Nault, J. D., and B. W. Karney. 2016a. "Adaptive hybrid transient formulation for simulating incompressible pipe network hydraulics." *J. Hydraul. Eng.* 142 (11): 04016050. https://doi.org/10.1061/(ASCE)HY.1943-7900.0001195.

Nault, J. D., and B. W. Karney. 2016b. "Improved rigid water column formulation for simulating slow transients and controlled operations." *J. Hydraul. Eng.* 142 (9): 04016025. https://doi.org/10.1061/(ASCE)HY.1943-7900.0001145.

Nicolet, C. 2007. "Hydroacoustic modelling and numerical simulation of unsteady operation of hydroelectric systems." Ph.D. thesis, Dept. of Mechanical Engineering, Swiss Federal Institute of Technology Lausanne.

Nicolet, C., B. Greiveldinger, J. J. Herou, B. Kawkabani, P. Allenbach, J. J. Simond, and F. Avellan. 2007. "High-order modeling of hydraulic power plant in islanded power network." *IEEE Trans. Power Syst.* 22 (4): 1870–1880. https://doi.org/10.1109/TPWRS.2007.907348.

Onizuka, K. 1981. "State space analysis of surges in large-scale branching pipeline systems." In Vol. 22 of *Bulletin of the faculty of agriculture*. Tokyo: Tokyo Univ. of Agriculture and Technology.

Onizuka, K. 1986. "System dynamics approach to pipe network analysis." *J. Hydraul. Eng.* 112 (8): 728–749. https://doi.org/10.1061/(ASCE)0733-9429(1986)112:8(728).

Prescott, S. L., and B. Ulanicki. 2003. "Dynamic modeling of pressure reducing valves." *J. Hydraul. Eng.* 129 (10): 804–812. https://doi.org/10.1061/(ASCE)0733-9429(2003)129:10(804).

© ASCE
04025054-13
J. Water Resour. Plann. Manage.

J. Water Resour. Plann. Manage., 2025, 151(10): 04025054

Prescott, S. L., and B. Ulanicki. 2008. "Improved control of pressure reducing valves in water distribution networks." *J. Hydraul. Eng.* 134 (1): 56–65. https://doi.org/10.1061/(ASCE)0733-9429(2008)134:1(56).

Shimada, M. 1989. "Graph-theoretical model for slow transient analysis of pipe networks." *J. Hydraul. Eng.* 115 (9): 1165–1183. https://doi.org/10.1061/(ASCE)0733-9429(1989)115:9(1165).

Shimada, M. 1992. "State-space analysis and control of slow transients in pipes." *J. Hydraul. Eng.* 118 (9): 1287–1304. https://doi.org/10.1061/(ASCE)0733-9429(1992)118:9(1287).

Simpson, A., J. Vítkovský, and M. Lambert. 2000. "Transients for calibration of pipe roughnesses using genetic algorithms." In *Proc., 8th Int. Conf. on Pressure Surges—Safe Design and Operation of Industrial Pipe Systems*, edited by A. Anderson, 587–597. London: Professional Engineering Publishing.

Souza, O. H., N. Barbieri, and A. H. M. Santos. 1999. "Study of hydraulic transients in hydropower plants through simulation of nonlinear model of penstock and hydraulic turbine model." *IEEE Trans. Power Syst.* 14 (4): 1269–1272. https://doi.org/10.1109/59.801883.

Ulanicki, B., and P. Beaujean. 2021. "Modeling dynamic behavior of water distribution systems for control purposes." *J. Water Resour. Plann. Manage.* 147 (8): 04021043. https://doi.org/10.1061/(ASCE)WR.1943-5452.0001403.

Vítkovský, J. P. 2001. "Inverse analysis and modelling of unsteady pipe flow: Theory, applications and experimental verification." Ph.D. thesis, School of Civil, Environmental and Mining Engineering, Univ. of Adelaide.

Xing, L., and L. Sela. 2020. "Transient simulations in water distribution networks: TSNet python package." *Adv. Eng. Software* 149 (Nov): 102884. https://doi.org/10.1016/j.advengsoft.2020.102884.

Zecchin, A. C. 2010. "Laplace-domain analysis of fluid line networks with applications to time-domain simulation and system parameter identification." Ph.D. thesis, School of Civil, Environmental and Mining Engineering, Univ. of Adelaide.

Zeng, W., N. Do, M. Lambert, J. Gong, B. Cazzolato, and M. Stephens. 2023. "Linear phase detector for detecting multiple leaks in water pipes." *Appl. Acoust.* 202 (Jan): 109152. https://doi.org/10.1016/j.apacoust.2022.109152.

Zeng, W., J. Gong, P. R. Cook, J. W. Arkwright, A. R. Simpson, B. S. Cazzolato, A. C. Zecchin, and M. F. Lambert. 2020. "Leak detection for pipelines using in-pipe optical fiber pressure sensors and a paired-IRF technique." *J. Hydraul. Eng.* 146 (10): 06020013. https://doi.org/10.1061/(ASCE)HY.1943-7900.0001812.

Zeng, W., J. Yang, and W. Guo. 2015. "Runaway instability of pump-turbines in S-shaped regions considering water compressibility." *J. Fluids Eng.* 137 (5): 051401. https://doi.org/10.1115/1.4029313.

Zeng, W., J. Yang, and W. Yang. 2016. "Instability analysis of pumped-storage stations under no-load conditions using a parameter-varying model." *Renewable Energy* 90 (May): 420–429. https://doi.org/10.1016/j.renene.2016.01.024.

Zeng, W., A. C. Zecchin, and M. F. Lambert. 2022. "Elastic water column model for hydraulic transient analysis of pipe networks." *J. Hydraul. Eng.* 148 (12): 04022027. https://doi.org/10.1061/(ASCE)HY.1943-7900.0002028.

Zhang, C., M. F. Lambert, J. Gong, A. C. Zecchin, A. R. Simpson, and M. L. Stephens. 2020. "Bayesian inverse transient analysis for pipeline condition assessment: Parameter estimation and uncertainty quantification." *Water Resour. Manage.* 34 (9): 2807–2820. https://doi.org/10.1007/s11269-020-02582-9.

© ASCE 04025054-14 J. Water Resour. Plann. Manage.

J. Water Resour. Plann. Manage., 2025, 151(10): 04025054